

Growth efficiency of dust aggregates through collisions with high mass ratios[★]

Koji Wada¹, Hidekazu Tanaka², Satoshi Okuzumi³, Hiroshi Kobayashi⁴, Toru Suyama⁵,
Hiroshi Kimura⁶, and Tetsuo Yamamoto⁷

¹ Planetary Exploration Research Center, Chiba Institute of Technology, 2-17-1 Tsudanuma, Narashino, 275-0016 Chiba, Japan
e-mail: wada@perc.it-chiba.ac.jp

² Institute of Low Temperature Science, Hokkaido University, 060-0819 Sapporo, Japan

³ Department of Earth and Planetary Sciences, Tokyo Institute of Technology, Meguro-ku, 152-8511 Tokyo, Japan

⁴ Department of Physics, Nagoya University, Nagoya, 464-8602 Aichi, Japan

⁵ Nagano City Museum, Hachimanpara Historical Park Ojimada-machi, 381-2212 Nagano, Japan

⁶ Graduate School of Science, Kobe University, c/o CPS (Center for Planetary Science), Chuo-ku Minatojima Minamimachi 7-1-48, 650-0047 Kobe, Japan

⁷ CPS (Center for Planetary Science), Kobe University, Chuo-ku Minatojima Minamimachi 7-1-48, 650-0047 Kobe, Japan

Received 11 July 2013 / Accepted 5 September 2013

ABSTRACT

Context. Collisional growth of dust aggregates is an essential process in forming planetesimals in protoplanetary disks, but disruption through high-velocity collisions (disruption barrier) could prohibit the dust growth. Mass transfer through very different-sized collisions has been suggested as a way to circumvent the disruption barrier.

Aims. We examine how the collisional growth efficiency of dust aggregates with different impact parameters depends on the size and the mass ratio of colliding aggregates.

Methods. We used an N -body code to numerically simulate the collisions of different-sized aggregates.

Results. Our results show that high values for the impact parameter are important and that the growth efficiency averaged over the impact parameter does not depend on the aggregate size, although the growth efficiency for nearly head-on collisions increases with size. We also find that the averaged growth efficiency tends to increase with increasing mass ratio of colliding aggregates. However, the critical collision velocity, above which the growth efficiency becomes negative, does not strongly depend on the mass ratio. These results indicate that icy dust can grow through high-velocity offset collisions at several tens of m s^{-1} , the maximum collision velocity experienced in protoplanetary disks, whereas it is still difficult for silicate dust to grow in protoplanetary disks.

Key words. planets and satellites: formation – protoplanetary disks – methods: numerical

1. Introduction

In protoplanetary disks, planetesimals are believed to be formed from dust aggregates consisting of submicron grains. Dust aggregates should grow through collisions, but its possibility is uncertain. One of the main problems is the existence of the disruption barrier, which is caused by collisions at velocities up to several tens of m s^{-1} in protoplanetary disks (e.g., Adachi et al. 1976; Weidenschilling & Cuzzi 1993; Dominik et al. 2007; Blum & Wurm 2008). Considering the minimum-mass solar nebula model of Hayashi (1981), the radial inward velocity of dust reaches 50 m s^{-1} owing to coupling with disk gas (Adachi et al. 1976; Weidenschilling & Cuzzi 1993; Suyama et al. 2008). Even if we assume a colder disk model (Kusaka et al. 1970; Chiang & Goldreich 1997; Chiang et al. 2001; Tanaka et al. 2005), the maximum radial inward velocity is still high, $\sim 25 \text{ m s}^{-1}$. In addition, the collision velocity would be increased by the influence of gas turbulence. For example, strong gas turbulence expressed by the α model with $\alpha = 0.01$ leads to velocity up to $\sim 100 \text{ m s}^{-1}$ (e.g., Cuzzi et al. 2001; Dominik et al. 2007).

Collisions between aggregates are directly simulated by N -body codes (e.g., Dominik & Tielens 1997; Paszun & Dominik 2009; Wada et al. 2009, 2011; Suyama et al. 2012; Seizinger & Kley 2013). We have been investigating the feasibility of dust growth at high-velocity collisions using an N -body code. In our simulations, fluffy aggregates represented by ballistic particle-cluster aggregation (BPCA) clusters are able to grow through collisions at velocities u_{col} up to $\sim 60 \text{ m s}^{-1}$ (averaged over the impact parameter) if they are of equal sizes and consist of icy particles with a radius $r = 0.1 \mu\text{m}$ (Wada et al. 2009). The BPCA structure is fairly compact (fractal dimension $D \sim 3$), compared to ballistic cluster-cluster aggregation (BCCA) structure ($D \lesssim 2$). Since dust aggregates are expected to be relatively compact thanks to collisional compression when they experience high-velocity collisions (Wada et al. 2008; Suyama et al. 2008) or to static compression by disk gas (Kataoka et al. 2013a,b), the growth and disruption process of BPCA clusters is particularly important for elucidating the formation process of planetesimals. Our results strongly support the formation model of icy planetesimals via direct dust growth (e.g., Okuzumi et al. 2012; Kataoka et al. 2013b).

However, the situation is much severe for silicate dust. Based on the numerical results of Wada et al. (2009), the critical collision velocity $u_{\text{col,crit}}$ for silicate aggregates is given by

[★] A complete set of our numerical results is available at the CDS via anonymous ftp to cdsarc.u-strasbg.fr (130.79.128.5) or via <http://cdsarc.u-strasbg.fr/viz-bin/qcat?J/A+A/559/A62>

$u_{\text{col,crit}} \approx 1.1 (r/0.76 \mu\text{m})^{-5/6} \text{ m s}^{-1}$. This is much less than the collision velocity achieved in protoplanetary disks. Our estimation on $u_{\text{col,crit}}$ for silicate aggregates is consistent with several laboratory experiments and numerical simulations for silicate aggregates (e.g., Blum & Wurm 2000, 2008; Langkowski et al. 2008; Güttler et al. 2010; Paszun & Dominik 2009; Seizinger & Kley 2013), suggesting the difficulty of silicate dust growth.

It should be noted that these results are obtained through collisions of equal-sized aggregates. In protoplanetary disks, however, collisions between different-sized dust aggregates generally would occur. As a result of numerical solutions of a coagulation equation (Smoluchowski equation) for dust growth with a realistic porosity model, Okuzumi et al. (2009) showed that collisions between different-sized dust aggregates are effective for fluffy dust to grow at an early growth stage and their prevailing mass ratio is ~ 10 (i.e., large dust is ten times heavier than small one). Collisions between less fluffy, similar-sized dust become dominant at the late stage. Such collisions broaden the size distribution of dust and the prevailing mass ratio is still as high as $\sim 3\text{--}5$ (Okuzumi et al. 2012).

Collisions between different-sized (mass) aggregates may increase $u_{\text{col,crit}}$ since large aggregates are expected to well absorb the impact energy of small aggregates. Smoothed particle hydrodynamic (SPH) simulations suggest the increase in the critical velocity for different-sized collisions (Meru et al. 2013). Laboratory experiments report that porous aggregates consisting of micron-sized SiO_2 particles can grow when they are collided onto large (flat) targets at $u_{\text{col}} > 10 \text{ m s}^{-1}$ (Wurm et al. 2005; Teiser & Wurm 2009; Paraskov et al. 2007). These experimental results suggest a positive effect of different-sized collisions on dust growth. They are obtained under head-on collisions alone, but head-on collisions are rare cases in nature. Numerical results of Wada et al. (2009) show that the critical collision velocity does not increase when offset collisions are taken into account. Teiser et al. (2011) report in their experiments that dust accretion efficiency decreases with increasing the impact angle θ , although their experiments are limited to $\theta < 45^\circ$. From another point of view, different-sized collisions may have an opposite effect producing much ejecta due to the injection of impact energy into a local region (Paszun & Dominik 2009). Therefore collisions between different-sized BPCA aggregates, including offset collisions, are worth investigating for discussion on dust growth. In addition, high-velocity collisions produce a large number of small aggregates as ejecta fragments (Paszun & Dominik 2009; Wada et al. 2009). Since ejecta would play an important role in dust growth and the total ejecta mass is a key to determine the mass loss rate through collisional cascades (Kobayashi & Tanaka 2010), we need a model of ejecta mass at high-velocity collisions of different-sized aggregates.

In this study, we carry out numerical simulations of collisions between icy BPCA clusters with various mass ratios (1, 16, and 64) to clarify the effect of collisions of different-sized aggregates on the critical collision velocity, taking into account offset collisions. In the next section we describe our numerical settings. The influence of different-sized collisions on the growth efficiency is presented in Sect. 3. Based on the numerical results, we discuss the feasibility of dust growth and the ejecta mass through the different-sized collisions in Sect. 4. Summary of this study is in Sect. 5.

2. Numerical model and settings

We performed 3D simulations of aggregate collisions with the numerical code developed in the previous papers (Dominik & Tielens 1997; Wada et al. 2007). We directly calculate the

motion of each particle, taking into account all mechanical interactions between particles in contact. The particle interaction model is based on the elastic contact theory with surface energy, which is the so-called JKR theory (Johnson et al. 1971; Johnson 1987; Chokshi et al. 1993; Dominik & Tielens 1995, 1996). Particles are elastic spheres with the same radius and have surface energy. The details of the interaction model are described in our previous paper (Wada et al. 2007). Here, we give a brief summary of our model. The contact theory of adhesive elastic spheres determines the interactions for each degree of motion (normal motion, sliding, rolling, and twisting). Energy dissipates at the moments of contact and separation of particles due to the excitation of elastic waves. When the displacements due to sliding, rolling, and twisting exceed their elastic limits, the mechanical energy is also dissipated. The amount of energy dissipation is proportional to the critical displacements.

In this study we simulate collisions between ice aggregates rather than silicate ones to save computational costs for a large number of simulation runs. The calculation time step is determined by using the equilibrium overlapping length between particles divided by the collision velocity. The overlapping length is defined as the distance $\delta = 2r - d$, where r is the particle radius and d is the distance between two particles' centers. The overlapping length changes, of course, as a function of time, but on average, it is the same order of magnitude as the equilibrium length $\delta_0 \propto (\gamma/\mathcal{E})^{2/3}$, with γ and \mathcal{E} being the surface energy and Young's modulus, respectively (the equilibrium state is achieved when attractive force by surface tension balances with repulsive force by elasticity without external force. See Wada et al. 2007 for more detail). The equilibrium length δ_0 for ice particles is larger than that for silicate by an order of magnitude, which validates our simulations for ice aggregates with a time step ten times longer than for silicate. Although we do not simulate collisions of silicate aggregates, we can estimate the behavior of silicate aggregates from results of ice ones. For example, the critical collision velocity for silicate aggregates can be estimated from that obtained for ice, according to scaling relations such as (Wada et al. 2009)

$$E_{\text{imp,crit}} \approx 30N_{\text{total}}E_{\text{break}}, \quad (1)$$

where $E_{\text{imp,crit}}$ is the critical impact energy for growth, E_{break} is the energy for breaking a single contact between two identical particles, and N_{total} is the total number of particles of two aggregates. Hence, particles in this study are spheres with the material properties of ice (the surface energy $\gamma = 100 \text{ mJ m}^{-2}$, Young's modulus $\mathcal{E} = 7 \text{ GPa}$, Poisson's ratio $\nu = 0.25$, and the material density $\rho = 1 \text{ g cm}^{-3}$) and the same radius $r = 0.1 \mu\text{m}$. The value of surface energy for ice particles is consistent with that measured in laboratory experiments (Gundlach et al. 2011). The critical rolling displacement is a free parameter and we fix it to be 10 \AA in this study.

Two colliding aggregates, projectiles and targets, are both BPCA clusters but they have different masses in the present study. The number of particles constituting projectiles, N_{proj} , is 500, 2000, or 8000, while that of targets, N_{target} , is 8000, 32 000, 128 000, or 512 000. Their sizes are approximately $1.5 \mu\text{m}$ (for $N = 500$), $2.4 \mu\text{m}$ (2000), $3.8 \mu\text{m}$ (8000), $4.8 \mu\text{m}$ (32 000), $7.7 \mu\text{m}$ (128 000), and $12 \mu\text{m}$ (512 000). Their porosity is almost the same as 86%, correspondent to the typical porosity of BPCA clusters. Using these aggregates, we examine collisions with the mass ratios $N_{\text{target}}/N_{\text{proj}} = 1, 16, \text{ or } 64$ (combinations of projectiles and targets are listed in Table 1). Figure 1 shows examples of initial aggregates with the mass ratio 16 and 64.

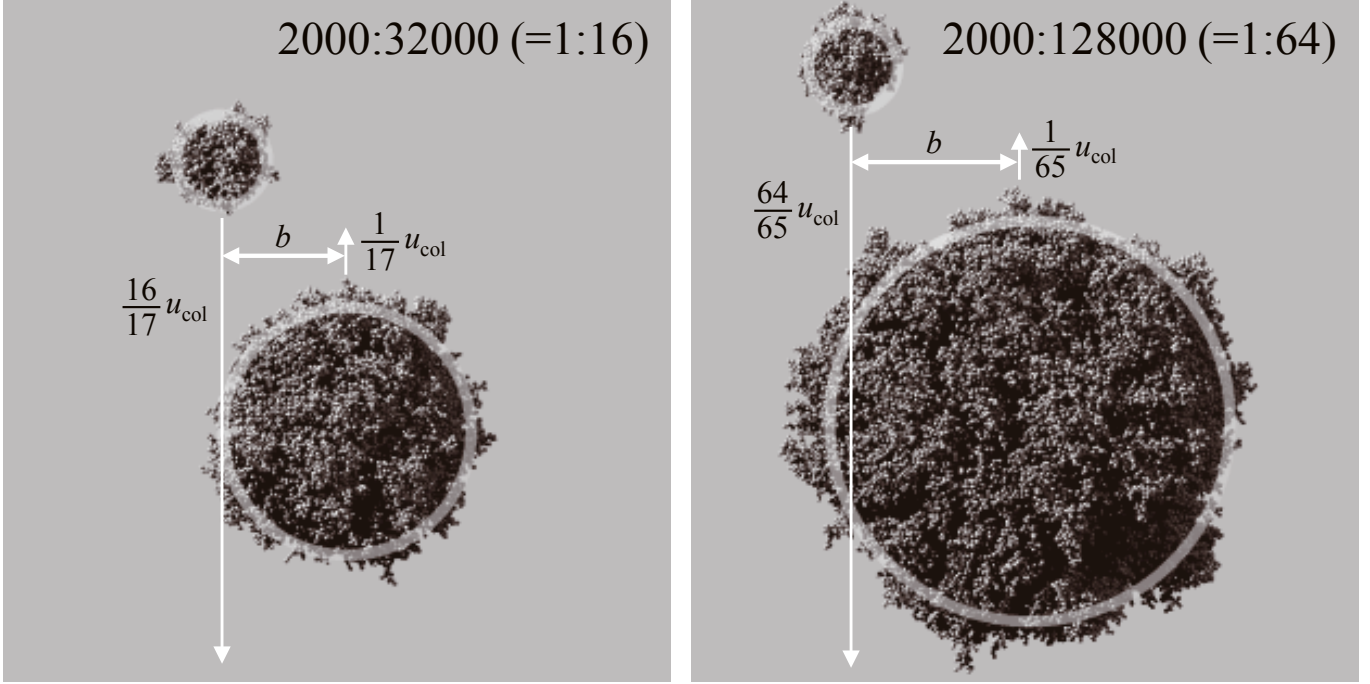


Fig. 1. Examples of initial BPCA clusters of the mass ratio $N_{\text{target}}/N_{\text{proj}} = 16$ ($N_{\text{target}} = 32\,000$ and $N_{\text{proj}} = 2000$, left) and $N_{\text{target}}/N_{\text{proj}} = 64$ ($N_{\text{target}} = 128\,000$ and $N_{\text{proj}} = 2000$, right). Each gray ring indicates the size of the characteristic radius of each aggregate. These aggregates collide with each other vertically at an impact parameter b with a relative velocity u_{col} . Here, the cases of $b = 0.69b_{\text{max}}$ are shown.

Table 1. Combinations of colliding aggregates and the obtained critical collision velocity averaged over the impact parameter

N_{proj}	N_{target}	$N_{\text{target}}/N_{\text{proj}}$	$u_{\text{col,crit}}$ [m s^{-1}]
8000	8000	1	68
2000	32 000	16	74
8000	128 000	16	67
500	32 000	64	74
2000	128 000	64	90
8000	512 000	64	72

For offset collisions, these aggregates are collided with various values of the impact parameter b , which is defined as the projected distance between the centers of mass of the aggregates in the direction perpendicular to the collision velocity. The maximum value of the impact parameter, b_{max} , is taken to be the sum of the characteristic radii of the projectile and the target, $r_{\text{c,proj}}$ and $r_{\text{c,target}}$,

$$b_{\text{max}} = r_{\text{c,proj}} + r_{\text{c,target}}. \quad (2)$$

The characteristic radius is defined by the radius of gyration of an aggregate multiplied by $\sqrt{5/3}$ and represents almost the apparent radius of BPCA cluster (Mukai et al. 1992, and see Fig. 1). Changing b value from 0 (head-on collision) to b_{max} (grazing collision), we see the influence of offset collisions and obtain numerical results averaged over b as described below in Eq. (4).

For each combination of different aggregate masses, we prepare three pairs of aggregates by randomly changing the sticking directions of particles that make up the aggregates, except for the target of $N_{\text{target}} = 512\,000$ only one type of which is prepared to save the computational time. Then, three runs for each case of the collision velocity and the impact parameter are carried out and their numerical results are averaged for discussion

except for the case of $N_{\text{target}} = 512\,000$ (all the numerical results of 972 runs are listed in the online table, available at the CDS). All points plotted in figures and the data shown in Table 1 of the present paper represent such averages. As the aggregates we treated in this study are BPCA clusters, their shape is almost spherical and there is no significant anisotropy between them. The equal-sized collisions (i.e., $N_{\text{target}}/N_{\text{proj}} = 1$) are already done in the previous paper (Wada et al. 2009), in which the critical rolling displacement was set to 8 \AA but their results would be almost the same as those with 10 \AA .

We examine the size and the mass-ratio dependencies of the collisional growth efficiency f defined by

$$f = (N_{\text{large}} - N_{\text{target}})/N_{\text{proj}}, \quad (3)$$

where N_{large} is the number of particles in the largest remnant in a collision. The growth efficiency counts how many particles, normalized by N_{proj} , are gained (or lost if the value is negative) for a target aggregate through a collision. The largest remnant mass represented by N_{large} is dependent on the impact parameter. The largest remnant mass averaged over the impact parameter, \bar{N}_{large} , is calculated as

$$\bar{N}_{\text{large}} = \frac{1}{\pi b_{\text{max}}^2} \int_0^{b_{\text{max}}} N_{\text{large}}(b) 2\pi b db = \int_0^1 N_{\text{large}} d(b/b_{\text{max}})^2 \quad (4)$$

and the averaged growth efficiency \bar{f} is given by $(\bar{N}_{\text{large}} - N_{\text{target}})/N_{\text{proj}}$. To see disruption of ice aggregates, the collision velocity u_{col} ranges from 6 to $\sim 500 \text{ m s}^{-1}$. In protoplanetary disks, the collision velocity for the size of dust aggregates simulated in our study must be much lower than those achieved for m-sized bodies, several tens m s^{-1} . However, our results are applicable for larger aggregates since our results are scaled in terms of the ratio of the kinetic energy density to the breaking energy for single contact, i.e., $u_{\text{col}}/\sqrt{E_{\text{break}}/m}$ – the aggregate size does not appear in this ratio – as shown later in

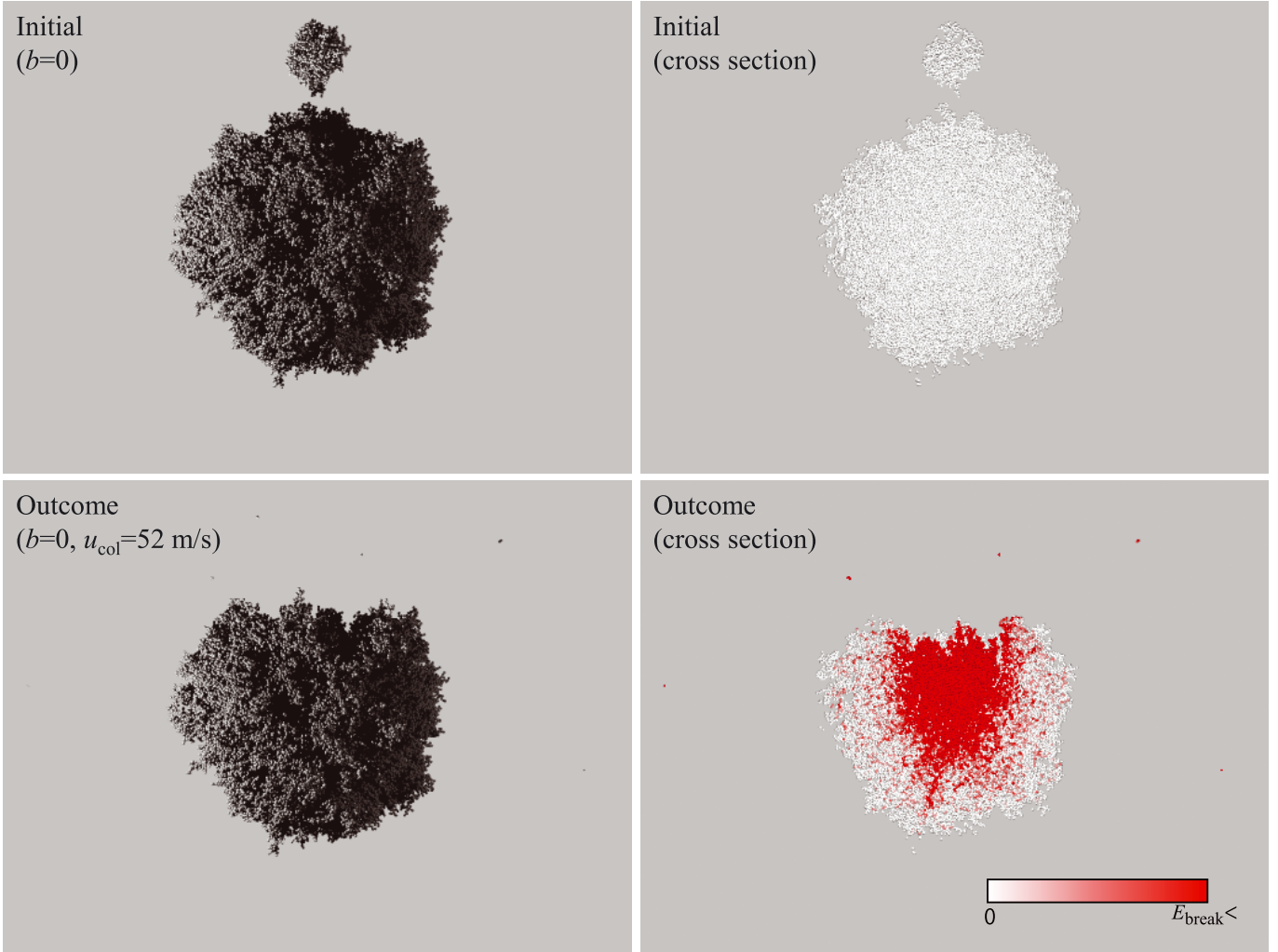


Fig. 2. Initial and final snapshots of a head-on collision ($b = 0$) between a projectile of $N_{\text{proj}} = 2000$ and a target of $N_{\text{target}} = 128\,000$ at $u_{\text{col}} = 52 \text{ m s}^{-1}$. *Right panels* show cross sectional views with particles that are painted dependent on the amount of energy dissipation as indicated in the scale bar.

Sect. 4.1. Wada et al. (2009) indicate that the growth efficiency averaged over b is independent of the aggregate size for equal-sized collisions in the range $f > 0$. In this study, therefore, we refer the equal-sized case only for $N_{\text{target}} = N_{\text{proj}} = 8000$ carried out in Wada et al. (2009).

3. Results

3.1. Snapshots

Figures 2 and 3 show examples of collisions between a projectile and a target with the mass ratio 64 ($N_{\text{target}} = 128\,000$ and $N_{\text{proj}} = 2000$). In both cases of head-on ($b = 0$) and offset ($b = 0.69b_{\text{max}}$) collisions, projectiles seem to be effectively captured by target aggregates even at high-velocity (52 m s^{-1}) collisions. At grazing impact ($b \simeq b_{\text{max}}$), the projectile passes by the target without major interaction, resulting in ejection of a small amount of fragments. As shown in cross sectional views of collision outcomes (right bottom panels of Figs. 2 and 3), the energy dissipation region is not distributed over whole target aggregates. This local dissipation mode is always observed in offset collisions and suggests that the collisional influence is limited to a region near the impact site, within a few times of a projectile size. In other words, the kinetic energy of the small projectile

can be efficiently absorbed by the target so that the projectile is almost completely captured even in this high-velocity case.

3.2. Growth efficiency

Figure 4 shows the growth efficiency $f = (N_{\text{large}} - N_{\text{target}})/N_{\text{proj}}$ as a function of the impact parameter for various sets of N_{target} and N_{proj} . High mass loss is observed with increasing collision velocities for each set. Figure 4a presents the results for the collisions of equal-sized aggregates. Head-on collisions ($b \sim 0$) result in high positive f values (i.e., mass gain) while collisions with higher b result in negative f (i.e., mass loss). With further increase in b , f converges to 0 since the projectiles interact with only a small part of the targets at grazing collisions.

The growth efficiency for offset collisions ($b^2 \gtrsim 0.1b_{\text{max}}^2$) mainly depends on the mass ratio (Figs. 4b–f). With increasing the mass ratio, the region of positive f becomes wider at each impact velocity. In contrast, no clear trend on the aggregate size is seen (cf., panels (b) and (c), or (e)–(f)).

In Fig. 5, we plot the growth efficiency \bar{f} averaged over b as a function of the impact velocity u_{col} for various sets of targets and projectiles. In both equal-mass and different-mass cases, \bar{f} decreases with increasing u_{col} and its transition from positive to negative occurs at $u_{\text{col,crit}} \simeq 80 \text{ m s}^{-1}$ ($u_{\text{col,crit}}$ for each case is

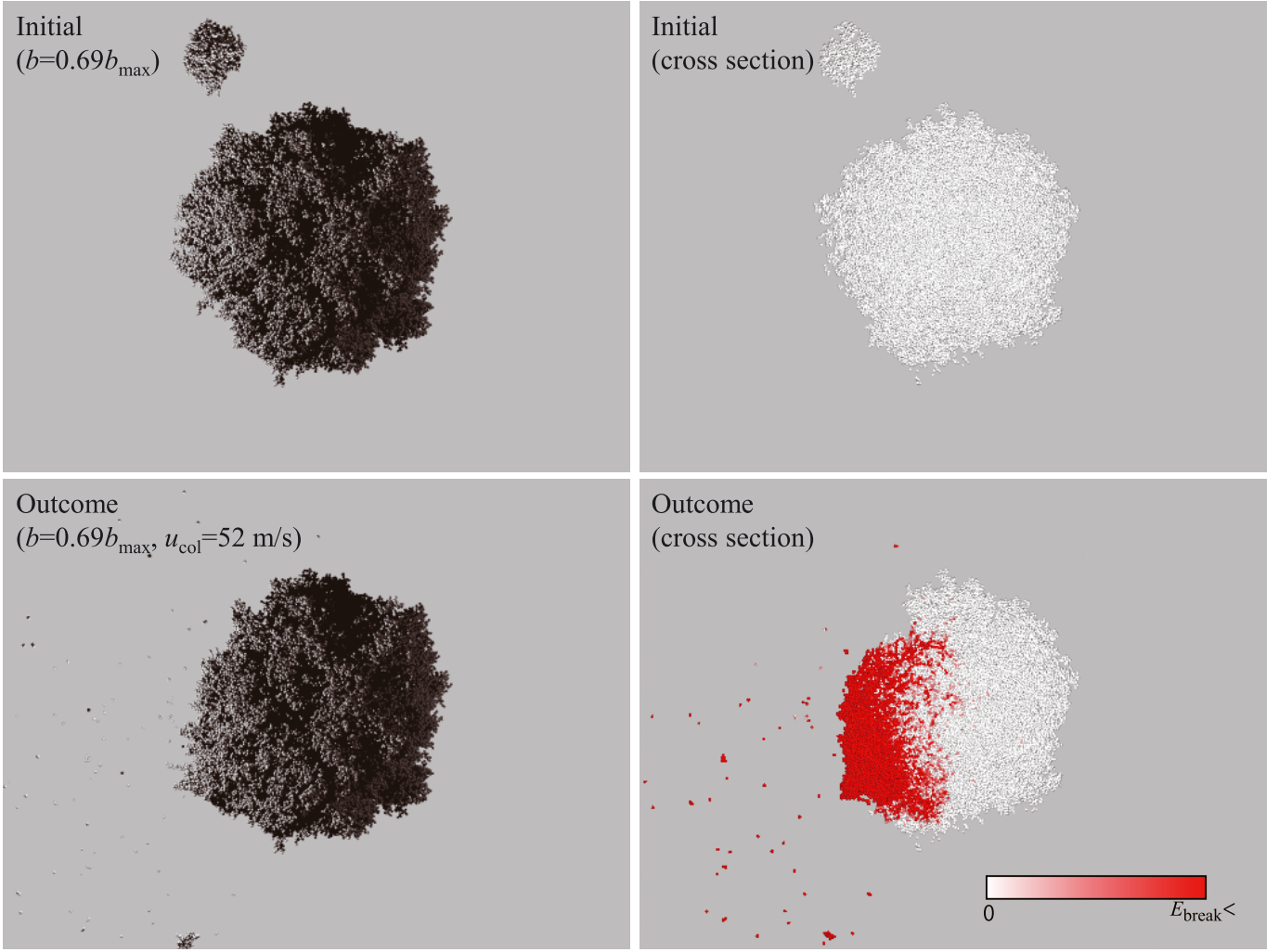


Fig. 3. Same as Fig. 2 but $b = 0.69b_{\max}$ (an offset collision).

listed in Table 1). This indicates that the maximum collision velocity for dust growth is almost independent of the mass ratio of two colliding aggregates. In the intermediate velocity region of $20 < u_{\text{col}} < 70 \text{ m s}^{-1}$, however, \bar{f} clearly increases with the mass ratio. That is, the high mass ratio helps dust growth at the intermediate collision velocities. Since any clear dependence on the aggregate size is not observed in Fig. 5, the above results are applicable to the cases with larger aggregates.

4. Discussion

4.1. Scaling formula of critical collision velocity

Here we consider a scaling relation giving $u_{\text{col,crit}}$ for different-sized collisions.

For equal-sized collisions, Wada et al. (2009) obtained a scaling relation on the critical impact energy for growth, $E_{\text{imp,crit}}$, given by Eq. (1). Based on the so-called JKR theory (e.g., Chokshi et al. 1993; Wada et al. 2007), E_{break} is given by

$$E_{\text{break}} \approx 23 \left[\gamma^5 r^4 (1 - \nu^2)^2 / \mathcal{E}^2 \right]^{1/3}. \quad (5)$$

Considering that $E_{\text{imp,crit}}$ at collisions of two identical aggregates is given by $1/2(N_{\text{total}}m/4)u_{\text{col,crit}}^2$ with m being the mass of one particle, the scaling relation (1) is transformed as

$$u_{\text{col,crit}} \approx 15 \sqrt{E_{\text{break}}/m}. \quad (6)$$

This gives $u_{\text{col,crit}} \approx 60 (r/0.1 \mu\text{m})^{-5/6} \text{ m s}^{-1}$ with the material properties of ice. When using the material properties of SiO_2 ($\gamma = 25 \text{ mJ m}^{-2}$, $\mathcal{E} = 54 \text{ GPa}$, $\nu = 0.17$, and $\rho = 2.6 \text{ g cm}^{-3}$), the above scaling relation gives $u_{\text{col,crit}}$ for silicate dust aggregates such as $u_{\text{col,crit}} \approx 6 (r/0.1 \mu\text{m})^{-5/6} \text{ m s}^{-1}$.

A scaling relation similar to that for equal-sized collisions, i.e., Eq. (6), is likely to hold in different-sized collisions because $u_{\text{col,crit}}$ is found to be independent of $N_{\text{target}} + N_{\text{proj}}$ and $N_{\text{target}}/N_{\text{proj}}$. From Fig. 5, in which the scale of the upper horizontal axis is indicated with $u_{\text{col}}/\sqrt{E_{\text{break}}/m}$, we have

$$u_{\text{col,crit}} \approx 20 \sqrt{E_{\text{break}}/m} \quad (7)$$

and this gives

$$u_{\text{col,crit}} \approx 80 \left(\frac{r}{0.1 \mu\text{m}} \right)^{-5/6} \text{ m s}^{-1} \quad (8)$$

for the material properties of ice. The factor in the above equations is slightly large compared to the equal-sized case (Eq. (6)). This may reflect the influence of the different-sized collisions.

4.2. Dust growth in protoplanetary disks

We found that aggregate collisions with high mass ratios $N_{\text{target}}/N_{\text{proj}}$ lead to high growth efficiency \bar{f} averaged over b .

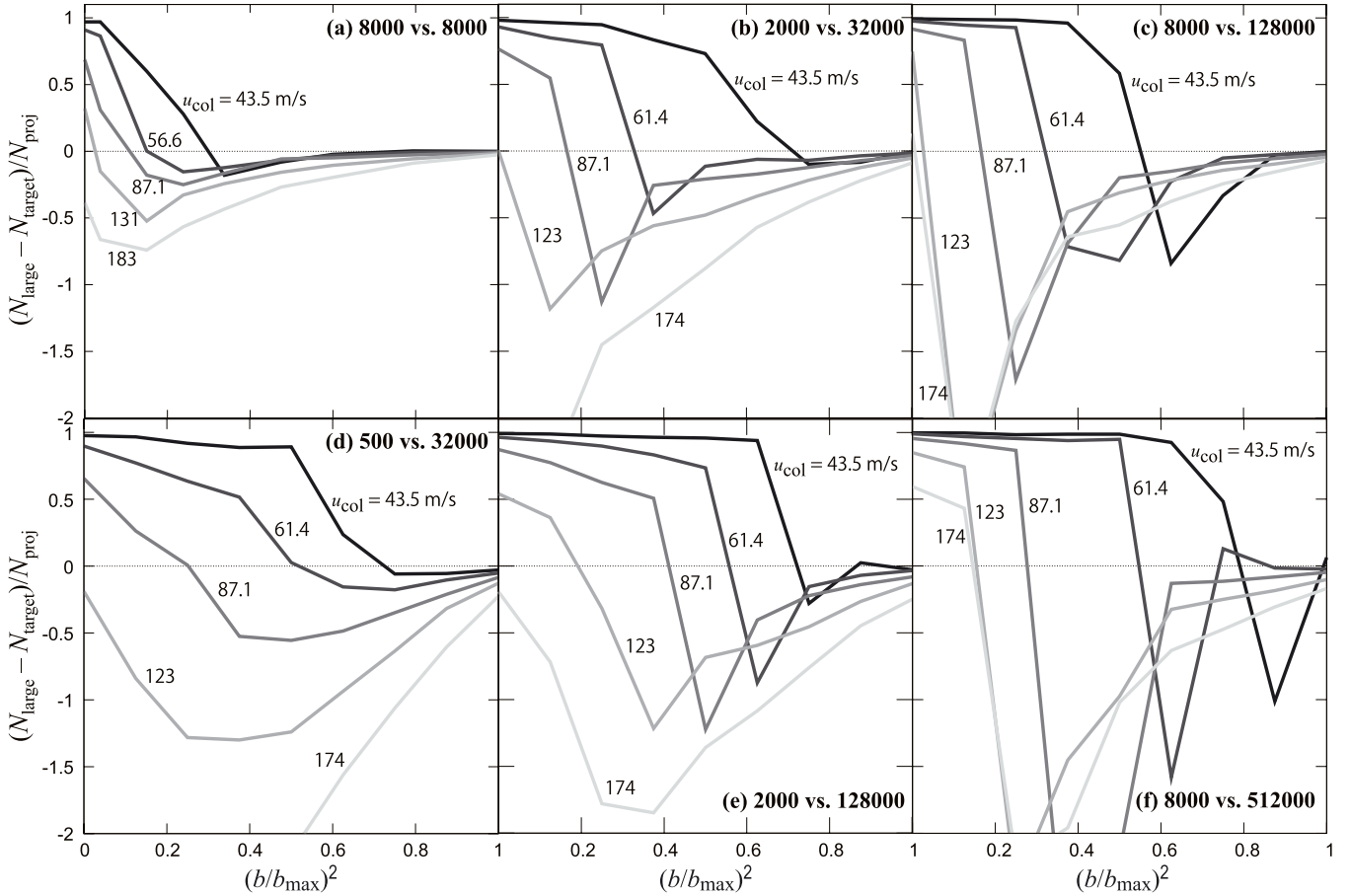


Fig. 4. Growth efficiency as a function of $(b/b_{\text{max}})^2$. Panels a–f) correspond to the cases of $(N_{\text{proj}}, N_{\text{target}}) = (8000, 8000)$, $(2000, 32000)$, $(8000, 128000)$, $(500, 32000)$, $(2000, 128000)$, and $(8000, 512000)$, respectively. Lines in each panel show results at various collision velocities indicated with numbers in m s^{-1} . Since the impact angle θ is related to b by $\sin \theta = b/b_{\text{max}}$, the horizontal axis can be read with $\sin^2 \theta$, instead of $(b/b_{\text{max}})^2$. Note that high negative values in the growth efficiency for strong mass-ratio collisions are due to normalization with N_{proj} and do not necessarily mean strong disruption of the targets.

The reason of this increase in \bar{f} would be explained by the effect of head-on collisions. Head-on collisions allow for aggregates to stick with each other more effectively than offset collisions (see Fig. 4). Experimental studies also report that head-on collisions of porous aggregates onto large (flat) targets result in high $u_{\text{col,crit}}$ (Wurm et al. 2005; Teiser & Wurm 2009; Paraskov et al. 2007). For high $N_{\text{target}}/N_{\text{proj}}$, offset collisions even at relatively high impact parameter b closely resemble head-on collisions, therefore producing high f . This effect promotes dust growth and planetesimal formation.

In contrast, averaging over the impact parameter, the critical collision velocity for dust growth is unchanged even for collisions with a high $N_{\text{target}}/N_{\text{proj}} = 64$ (the critical velocity for ice aggregates is less than 100 m s^{-1}). One reason for this suppression is that offset collisions, at which ejected mass becomes high, partly contribute to suppress the increase in $u_{\text{col,crit}}$. Another and probably main reason is that only the kinetic energy or the velocity of the projectile is important for the growth efficiency when the target size is sufficiently large. This is suggested by the fact that the impact energy is not distributed over a whole region of a target, limited to a region comparable to the projectile size (Figs. 2 and 3). The collision outcomes would be similar to cratering when the target size is sufficiently large.

As shown above, icy aggregates have sufficiently high $u_{\text{col,crit}}$ and the growth efficiency is significantly enhanced at $u_{\text{col}} \sim 50 \text{ m s}^{-1}$ for collisions with high mass ratios. These strongly

support the formation model of icy planetesimals via direct dust growth (e.g., Okuzumi et al. 2012; Kataoka et al. 2013b). For silicate dust aggregates, on the other hand, the critical velocity for growth is estimated to be $8 (r/0.1 \mu\text{m})^{-5/6} \text{ m s}^{-1}$ from the scaling relation (Eq. (7)). Since the collision velocity in protoplanetary disks could reach at least 25 m s^{-1} , $u_{\text{col,crit}} \approx 8 \text{ m s}^{-1}$ means that silicate aggregates cannot grow through collisions. In contrast, the optimistic growth possibility with $u_{\text{col,crit}} > 20 \text{ m s}^{-1}$ is inferred from experimental studies (Wurm et al. 2005; Teiser & Wurm 2009; Teiser et al. 2011; Paraskov et al. 2007). In these experiments, however, aggregate accretion is argued based on (nearly) head-on collisions. Head-on collisions tend to increase the growth efficiency and we can see the trend in Fig. 4, focusing on f values at $b = 0$. For example, in panel (f), f around $b = 0$ is still positive at $u_{\text{col}} = 174 \text{ m s}^{-1}$ and $u_{\text{col,crit}}$ reaches more than twice compared to that in Eq. (8). In addition, comparing panels (d), (e), and (f), $u_{\text{col,crit}}$ at $b = 0$ increases with increasing the aggregate size. This trend is also shown at equal-mass collisions (Wada et al. 2009). When we extrapolate this trend, head-on collisions of larger aggregates would make $u_{\text{col,crit}}$ higher and explain the high $u_{\text{col,crit}} > 20 \text{ m s}^{-1}$ measured in the experiments. For dust aggregates in protoplanetary disks, however, offset collisions are dominant rather than head-on collisions and collisions with the impact parameter $b^2 > 0.5b_{\text{max}}^2$ (the impact angle $\theta > 45^\circ$) become important. Including offset collisions the increase in $u_{\text{col,crit}}$ would not be significant as shown in

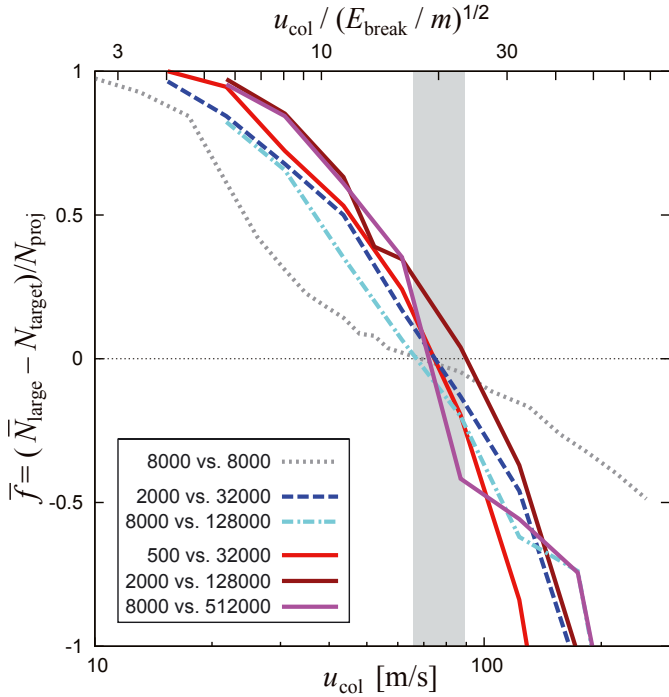


Fig. 5. Growth efficiency averaged over b as a function of u_{col} for collisions with various combinations of N_{proj} and N_{target} . The shadow region of $u_{\text{col}} = 67\text{--}90\text{ m s}^{-1}$ indicates the critical collision velocities. The scale of the upper horizontal axis is given by $u_{\text{col}}/\sqrt{E_{\text{break}}/m}$, where E_{break} is the energy for breaking a single contact and m is the monomer mass.

the present study. Therefore, silicate dust is still difficult to grow in protoplanetary disks, in which the collision velocity becomes up to several tens of m s^{-1} .

4.3. Total ejecta mass

As discussed above, the net dust growth needs the condition $f > 0$, namely how the target or the largest remnant can survive and grow through collisions. On the other hand, small fragments or ejecta produced during collisions of dust and planetesimals would also play an important role in protoplanetary disks. For example, since the observationally-indicated lifetime of small grains are much longer than the collisional growth timescale of grains, small grains resulting from collisional fragmentation of growing grains are required to explain the dust retention in protoplanetary disks (e.g., Birnstiel et al. 2009). In addition, debris disks, gas-poor disks around stars with ages older than several million years, are composed of small grains supplied from collisional fragmentation of large bodies. The fragment production rate is mainly determined by the total ejecta mass M_{ej} defined by $N_{\text{target}} + N_{\text{proj}} - N_{\text{large}}$ (Kobayashi & Tanaka 2010). Therefore, we investigate the total ejecta mass normalized by the projectile mass M_{proj} ($= N_{\text{proj}}$), i.e., $M_{\text{ej}}/M_{\text{proj}}$ ($= 1 - f$) against the collision velocity.

We plot the total ejecta mass \bar{M}_{ej} averaged over the impact parameter, normalized by the mass of a projectile, M_{proj} , as a function of u_{col} (Fig. 6). Since $M_{\text{ej}}/M_{\text{proj}}$ is calculated by $1 - f$, Fig. 6 is another expression of Fig. 5. We find a trend that $\bar{M}_{\text{ej}}/M_{\text{proj}}$ is roughly proportional to u_{col} for various combinations of N_{proj} and N_{target} although $\bar{M}_{\text{ej}}/M_{\text{proj}}$ deviates from that trend for low collision velocities. In Fig. 6, we plot a line

$$\bar{M}_{\text{ej}}/M_{\text{proj}} = u_{\text{col}}/u_{\text{col,crit}}, \quad (9)$$

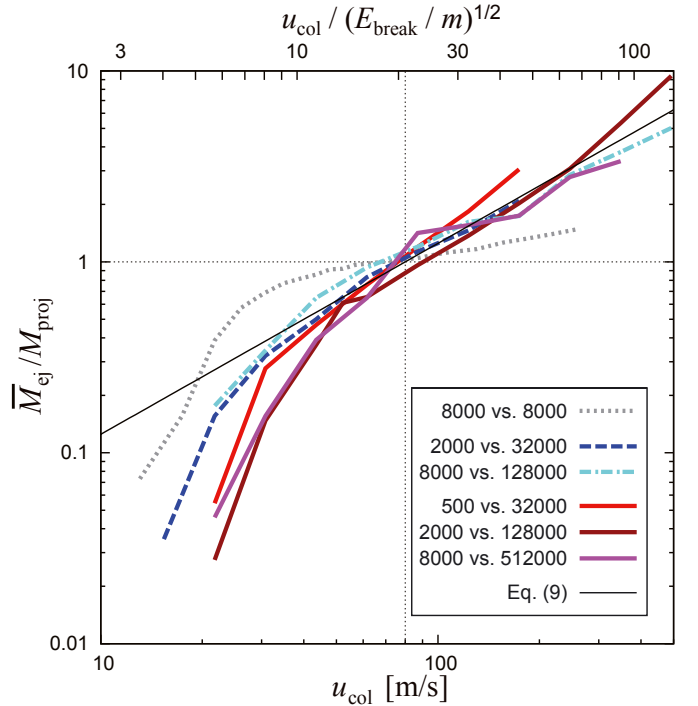


Fig. 6. Total ejecta mass averaged over b as a function of u_{col} for collisions with various combinations of N_{proj} and N_{target} . The thin solid line denotes equation (9). The scale of the upper horizontal axis is given by $u_{\text{col}}/\sqrt{E_{\text{break}}/m}$.

where $u_{\text{col,crit}}$ is given by 80 m s^{-1} . This formula roughly accounts for the data in the range $u_{\text{col}} > 20\text{ m s}^{-1}$. In the lower range $u_{\text{col}} < 20\text{ m s}^{-1}$, M_{ej} is significantly low compared to the formula. According to a scaling relation on the cratering process (Housen & Holsapple 2011), ejecta mass produced in cratering on sand targets is scaled with the projectile momentum, i.e., $M_{\text{ej}} \propto M_{\text{proj}}u_{\text{col}}$. Therefore, collisions between different-sized aggregates can be interpreted as a cratering process in dissipative media.

For studies on the fragmentation production rate in debris disks, it is common to introduce the specific energy Q_D^* , which is needed to break and eject the half mass of colliding bodies. From Eq. (9) and the fragmentation model by Kobayashi & Tanaka (2010), we obtain

$$Q_D^* \simeq u_{\text{col}}u_{\text{col,crit}}/2 = 4000\text{ J kg}^{-1} \left(\frac{u_{\text{col}}}{100\text{ m s}^{-1}} \right) \left(\frac{r}{0.1\text{ }\mu\text{m}} \right)^{-5/6} \quad (10)$$

for ice aggregates. Note that we obtain the formula under the assumption of unbreakable monomers and hence Eq. (10) is valid for $u_{\text{col}} \lesssim 1\text{ km s}^{-1}$. In debris disks, u_{col} is almost independent of the grain mass and the collisional fragmentation dominates for grains influencing disk luminosities. This situation allows for collisional cascades to determine the mass distribution of such grains. Since Q_D^* is independent of M_{proj} , the differential number density is proportional to $M^{-11/6}$ with M being grain mass (Kobayashi & Tanaka 2010). This mass dependence is the same as the classical theory of collisional cascade (Dohnanyi 1969; Tanaka et al. 1996). For protoplanetary disks, u_{col} is not determined as simply as that for debris disks. Collisions between small particles have $u_{\text{col}} \ll u_{\text{col,crit}}$, while u_{col} is close to $u_{\text{col,crit}}$ for collisions with large particles (e.g., Ormel & Cuzzi 2007).

Numerically solving the Smoluchowski equation (e.g., Okuzumi et al. 2012; Kobayashi et al. 2010) coupling with our result for fragmentation would be necessary to clarify the grain mass distribution in protoplanetary disks.

5. Summary

From a point of view of the dust growth through collisions in protoplanetary disks, in particular how dust can circumvent the disruption barrier, it is important to reveal whether or not the high-velocity collisions between different-sized aggregates affect the dust growth, not only in the case of head-on collisions but also in offset collisions. We investigate the collisions of icy aggregates with various sizes, mass ratios, and impact parameters, using our N -body code simulations. As a result, our findings are as follows:

- The growth efficiency $f = (N_{\text{large}} - N_{\text{target}})/N_{\text{proj}}$ decreases from positive to negative with increasing the impact parameter b , but its positive region is stretched with increasing the mass ratio $N_{\text{target}}/N_{\text{proj}}$. Owing to this trend, the growth efficiency averaged over b is significantly enhanced at intermediate velocities $20 < u_{\text{col}} < 70 \text{ m s}^{-1}$, for collisions with high mass ratios. This promotes the formation of icy planetesimals via direct dust growth.
- On the other hand, the high mass ratio does not affect significantly the critical collision velocity $u_{\text{col,crit}}$ for dust growth. We show that $u_{\text{col,crit}}$ results in around 80 m s^{-1} almost independent on the size and the mass ratio. We obtain a scaling relation

$$u_{\text{col,crit}} \simeq 20 \sqrt{E_{\text{break}}/m} \quad (11)$$

with E_{break} being the breaking energy for a pair of particles in contact and m the monomer mass. From this scaling relation, we obtain

$$u_{\text{col,crit}} = \begin{cases} 80 (r/0.1 \mu\text{m})^{-5/6} & \text{for ice} \\ 8 (r/0.1 \mu\text{m})^{-5/6} & \text{for silicate.} \end{cases} \quad (12)$$

- It should be noted that $u_{\text{col,crit}}$ for head-on collisions reaches more than twice that given in the above equations. However, if the realistic averaging over the impact parameter is done, offset collisions are dominant and head-on collisions does not contribute to the increase in $u_{\text{col,crit}}$.
- The total ejecta mass $M_{\text{ej}} = N_{\text{target}} + N_{\text{proj}} - N_{\text{large}}$ is also examined in our simulations. We obtain a scaling relation on the ejecta mass \bar{M}_{ej} averaged over the impact parameter b for relatively high $u_{\text{col}} > 20 \text{ m s}^{-1}$ as

$$\bar{M}_{\text{ej}} = M_{\text{proj}} \frac{u_{\text{col}}}{u_{\text{col,crit}}}. \quad (13)$$

This indicates that the total ejecta mass is determined by the projectile's momentum. Combining this scaling relation with the fragmentation model of Kobayashi & Tanaka (2010), we also obtain a formula of the specific energy for ejecting the half mass of colliding bodies, Q_D^* , as

$$Q_D^* \simeq u_{\text{col}} u_{\text{col,crit}}/2. \quad (14)$$

Applying the above scaling relation to aggregates consisting of silicate particles with a radius of $0.1 \mu\text{m}$, $u_{\text{col,crit}}$ results

in only 8 m s^{-1} , less than the collision velocity achieved in protoplanetary disks. Although icy dust can grow through collisions and the different mass ratio helps the dust growth, another factor in dust aggregate collisions should be considered to increase the feasibility of silicate dust growth for planetesimal formation.

Acknowledgements. We thank the reviewer, Prof. Stuart Weidenschilling, for helpful comments that improved this paper. We are grateful to Dr. Takeshi Chigai for technical support on computer setup. This study was supported by the Grants-in-Aid from JSPS (21340040, 22740299, 24540459) and MEXT (23103005).

References

- Adachi, I., Hayashi, C., & Nakazawa, K. 1976, *Prog. Theor. Phys.*, 56, 1756
- Birnstiel, T., Dullemond, C. P., & Brauer, F. 2009, *A&A*, 503, L5
- Blum, J., & Wurm, G. 2000, *Icarus*, 143, 138
- Blum, J., & Wurm, G. 2008, *ARA&A*, 46, 21
- Chiang, E. I., & Goldreich, P. 1997, *ApJ*, 490, 368
- Chiang, E. I., Joungh, M. K., Creech-Eakman, M. J., et al. 2001, *ApJ*, 547, 1077
- Chokshi, A., Tielens, A. G. G. M., & Hollenbach, D. 1993, *ApJ*, 407, 806
- Cuzzi, J. N., Hogan, R. C., Paque, J. M., & Dobrovolskis, A. R. 2001, *ApJ*, 546, 496
- Dominik, C., & Tielens, A. G. G. M. 1995, *Phil. Mag. A*, 72, 783
- Dominik, C., & Tielens, A. G. G. M. 1996, *Phil. Mag. A*, 73, 1279
- Dominik, C., & Tielens, A. G. G. M. 1997, *ApJ*, 480, 647
- Dominik, C., Blum, J., Cuzzi, J. N., & Wurm, G. 2007, in *Protostars and Planets V*, eds. B. Reipurth, D. Jewitt, & K. Kei (Tucson: University of Arizona Press), 783
- Dohnanyi, J. S. 1969, *J. Geophys. Res.*, 74, 2431
- Gundlach, B., Kiliyas, S., Beitz, E., & Blum, J. 2011, *Icarus*, 214, 717
- Güttler, C., Blum, J., Zsom, A., Ormel, C. W., & Dullemond, C. P. 2010, *A&A*, 513, A56
- Hayashi, C. 1981, *Prog. Theor. Phys. Suppl.*, 70, 35
- Housen, K. R., & Holsapple, K. A. 2011, *Icarus*, 211, 856
- Johnson, K. L. 1987, *Contact Mechanics* (Cambridge: Cambridge Univ. Press)
- Johnson, K. L., Kendall, K., & Roberts, A. D. 1971, *Proc. R. Soc. London A*, 324, 301
- Kataoka, A., Tanaka, H., Okuzumi, S., & Wada, S. 2013a, *A&A*, 554, A4.
- Kataoka, A., Tanaka, H., Okuzumi, S., & Wada, S. 2013b, *A&A*, 557, L4.
- Kobayashi, H., & Tanaka, H. 2010, *Icarus*, 206, 735
- Kobayashi, H., Tanaka, H., Krivov, A. V., & Inaba, S. 2010, *Icarus*, 209, 836
- Kusaka, T., Nakano, T., & Hayashi, C. 1970, *Prog. Theor. Phys.*, 44, 1580
- Langkowski, D., Teiser, J., & Blum, J. 2008, *ApJ*, 675, 764
- Meru, F., Geretshauser, R. J., Speith, R., & Kley, W. 2013, *MNRAS*, in press
- Mukai, T., Ishimoto, H., Kozasa, T., Blum, J., & Greenberg, J. M. 1992, *A&A*, 262, 315
- Okuzumi, S., Tanaka, H., & Sakagami, M.-a. 2009, *ApJ*, 707, 1247
- Okuzumi, S., Tanaka, H., Kobayashi, H., & Wada, K. 2012, *ApJ*, 752, 106
- Ormel, C. W., & Cuzzi, J. N. 2007, *A&A*, 466, 413
- Paraskov, G. B., Wurm, G., & Krauss, O. 2007, *Icarus*, 191, 779
- Paszun, D., & Dominik, C. 2009, *A&A*, 507, 1023
- Seizinger, A., & Kley, W. 2013, *A&A*, 551, A65
- Suyama, T., Wada, K., & Tanaka, H. 2008, *ApJ*, 684, 1310
- Suyama, T., Wada, K., Tanaka, H., & Okuzumi, S. 2012, *ApJ*, 753, 115
- Tanaka, H., Inaba, S., & Nakazawa, K. 1996, *Icarus*, 123, 450
- Tanaka, H., Himeno, Y., & Ida, S. 2005, *ApJ*, 625, 414
- Tanaka, H., Wada, K., Suyama, T., & Okuzumi, S. 2012, *Prog. Theor. Phys. Suppl.*, 195, 101
- Teiser, J., & Wurm, G. 2009, *MNRAS*, 393, 1584
- Teiser, J., Küpper, M., & Wurm, G. 2011, *Icarus*, 215, 596
- Wada, K., Tanaka, H., Suyama, T., Kimura, H., & Yamamoto, T. 2007, *ApJ*, 661, 320
- Wada, K., Tanaka, H., Suyama, T., Kimura, H., & Yamamoto, T. 2008, *ApJ*, 677, 1296
- Wada, K., Tanaka, H., Suyama, T., Kimura, H., & Yamamoto, T. 2009, *ApJ*, 702, 1490
- Wada, K., Tanaka, H., Suyama, T., Kimura, H., & Yamamoto, T. 2011, *ApJ*, 737, 36
- Weidenschilling, S. J., & Cuzzi, J. N. 1993, in *Protostars and Planets III*, eds. E. H. Levy, & J. I. Lunine (Tucson: University of Arizona Press), 1031
- Wurm, G., Paraskov, G., & Krauss, O. 2005, *Icarus*, 178, 253